Physics of Semiconductors.
Defects in the crystal structure

UDC 538.9

EDN ZDGBEQ
https://www.doi.org/10.33910/2687-153X-2024-5-4-215-220

Calculation of the formation energy and transformation probabilities of some intrinsic defects in hexagonal boron nitride

I. I. Yanibekov ✉[1], Yu. V. Petrov [1]

[1] Saint Petersburg State University, 7/9 Universitetskaya Emb., Saint Petersburg 199034, Russia

Authors

Iskander I. Yanibekov, ORCID: 0009-0003-4400-0168, e-mail: iskander1331@mail.ru

Yuri V. Petrov, ORCID: 0000-0003-3084-3677, e-mail: y.petrov@spbu.ru

For citation: Yanibekov, I. I., Petrov, Yu. V. (2024) Calculation of the formation energy and transformation probabilities of some intrinsic defects in hexagonal boron nitride. *Physics of Complex Systems*, 5 (4), 215–220. https://www.doi.org/10.33910/2687-153X-2024-5-4-215-220 EDN ZDGBEQ

Received 28 August 2024; reviewed 11 October 2024; accepted 11 October 2024.

Funding: The research is supported by the Russian Science Foundation, project No. 23-22-00067.

Abstract. Hexagonal boron nitride (h-BN) is of interest due to its potential use in electronics and, in particular, the fabrication of single-photon emitters. In this paper, some properties of defects, namely, a boron vacancy (V_B) and an anti-site complex with a nitrogen vacancy (N_BV_N) in various charge states are studied. The energies of defect formation are calculated using density functional theory (DFT). Probabilities of transitions between them are estimated, and the annealing temperatures required for the transformation of h-BN are calculated.

Keywords: defects in hexagonal boron nitride, DFT, boron vacancy, anti-site nitrogen vacancy complex, defect transformation

Introduction

Hexagonal boron nitride (h-BN) is currently used as a material for dielectric substrates in electronics (Dean et al. 2010) and high-frequency devices (Pazos et al. 2024), and is considered as a promising candidate for single-photon emitters for quantum cryptography. It has a hexagonal structure and a band gap of about 6 eV (Cassabois et al. 2016).

One of the variants of single-photon sources can be an anti-site complex with a nitrogen vacancy (N_BV_N) (Liu et al. 2024; Tran et al. 2016). At the moment, there are several works (Grosso et al. 2017; Venturi et al. 2024) devoted to the methods of fabricating N_BV_N by irradiating a sample with helium ions with V_B formation and subsequent annealing, but the modeling of the V_B–N_BV_N transformation process has not been published yet.

The purpose of this work is to calculate the formation energies of V_B and N_BV_N vacancies in various charge states by means of DFT and to determine which of them is the most energetically favorable under given conditions, as well as finding the energy barriers required to transform one type of a defect into another.

Methods

In this paper, we perform calculations of h-BN energy using a density functional theory (DFT) approach. The structure was simulated using the ASE software package (Larsen et al. 2017). First, we created a h-BN supercell consisting of 4 layers with a total number of 128 atoms and hexagonal lattice constants a = 2.5 and c = 6.65 (Fig. 1 (a)). Then we obtained the required defect types by removing and moving atoms (Fig. 1 (b, c)).

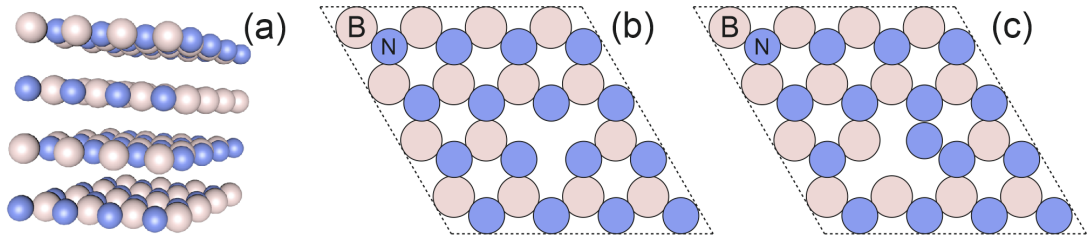

Fig. 1. (a) General side view of the modeled structure; (b) schematic representation of the first layer of the simulated structure with a V_B defect; (c) schematic representation of the first layer of the simulated structure with a $N_B V_N$ defect

The energy was calculated using the GPAW energy calculator (Mortensen et al. 2024) with the following parameters: periodic boundary conditions in all directions, plane wave basis (PW) and PBE exchange-correlation functional (Perdew et al. 1996). The calculation was performed for 2 special points in the Brillouin zone, namely Γ and M. The Kohn–Sham orbitals occupations determined using the Fermi–Dirac function with kT = 25 meV, corresponding to room temperature. Then, the structure was optimized using the MDMin method (Verlet method modification) by minimizing the energy using the minimum of the forces between atoms.

When calculating the energies for different charge states, the charges were added to the GPAW calculator, and the resulting electrostatic corrections, which will be discussed below, were taken into account during the final energy calculation.

After optimizing the structures, we calculated the defect energy taking into account its charge using the following formula (Weston et al. 2018):

$$E_{def}(E_F) = E_{dfull} - E_{h-BN} - \mu_B - E_{elc}[q] + q(\Delta V + E_F) \quad (1)$$

where E_{dfull} — full energy of the structure with a defect after optimization, E_{h-BN} — full energy of the structure without defects, $\mu_B = 2{,}9\ eV$ — chemical potential of Boron (Weston et al. 2018), $E_{elc}[q]$ — electrostatic correction, q — defect charge, E_F — Fermi energy, and ΔV — parameter required to align the electrostatic potential of the defect-containing supercell with the electrostatic potential of a pristine supercell. Its value is a function of the distance from the defect and has to be selected from an area located far from the defect (Freysoldt et al. 2011).

The chemical potential of Boron μ_B can be 0 eV or 2.9 eV depending on the conditions of growth: B-poor or N-poor correspondingly (Weston et al. 2018). However, this choice does not play a significant role not only in the calculation of the barriers, but also in comparing the formation energies, since it leads to the same shift of the zero level of the formation energies for both types of defects considered.

Then, using the energies of defect formation as edge points, we calculated the energy barriers of the transitions between defects using the Nudged Elastic Band (NEB) method (Lindgren et al. 2019) with 8 intermediate points between the initial and final positions of atoms in the supercell.

Knowing the values of the transition barrier energies, we calculated the transition probabilities at room temperature using (Weston et al. 2018):

$$\Gamma = \Gamma_0 \exp\left(-\frac{E_b}{k_b T}\right) \quad (2)$$

where $\Gamma_0 = 10^{14}\, s^{-1}$ h-BN phonon frequency (Geick et al. 1966), E_b — transition barrier, k_b — Boltzmann constant, and T — temperature.

Then we estimated the annealing temperature corresponding to $\Gamma = 1 s^{-1}$:

$$T = \frac{-E_b}{k_b \ln\left(\frac{\Gamma}{\Gamma_0}\right)} \quad (3)$$

It is also worth noting that the annealing temperature is not so sensitive to the choice of the constant Γ_0 because of the logarithmic dependence in (3).

 https://www.doi.org/10.33910/2687-153X-2024-5-4-215-220

Results and discussion

After the structural optimization we calculated the maximum atom displacements relative to the lattice sites in an ideal crystal, and for neutral defects they were of 0.075 Å for V_B and 0.045 Å for N_BV_N. These values are two orders of magnitude smaller than the lattice constants, and their detailed analysis is beyond the scope of this study.

Based on the obtained defect formation energies, we can plot the dependence of the defect formation energy on the Fermi level in various charge states (Fig. 2). As it can be seen from (1), when the defect is neutral ($q = 0$), there is no dependence of the defect formation energy on the Fermi level within the band gap. These states correspond to the horizontal solid red and black lines in (Fig. 2).

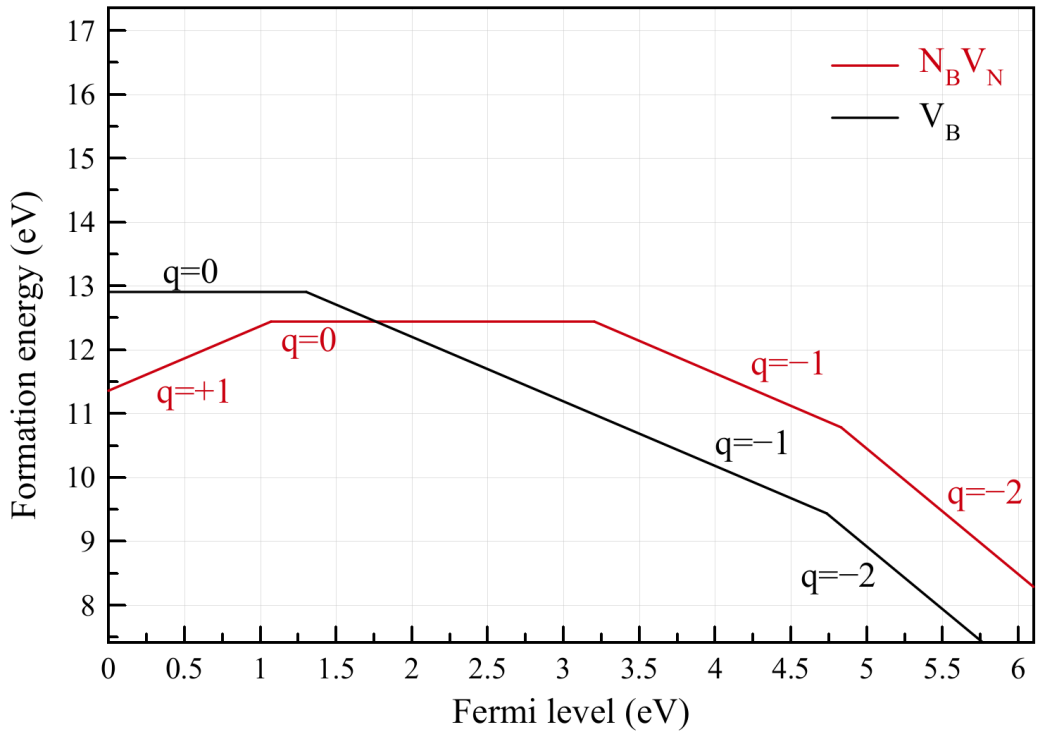

Fig. 2. Dependences of the defect formation energy on the Fermi level in different charge states

Table 1 presents the ranges of Fermi level values at which certain charge states are energetically more favorable for each type of defect, as well as the transition points between charge states. The red curve in (Fig. 2), corresponding to V_B, intersects with the black curve N_BV_N at a Fermi level of 1.75 eV and a formation energy of 12.9 eV.

Table 1. The most energetically favorable defect charges depending on the Fermi level

Charge of defect	V_B		N_BV_N	
	Fermi level, eV	Transition point, eV	Fermi level, eV	Transition point, eV
+1	–	–	0–1	12.4
0	0–1.25		1–3.2	
–1	1.25–4.75	12,9	3.2–4.8	12.4
–2	4.75–6	9,4	4.8–6	10.9

For further analysis, we will consider an intrinsic semiconductor, and therefore, focus on the transitions with the Fermi level near the center of the band gap. Thus, according to (Fig. 2), in the intrinsic h-BN, the boron vacancy V_B in the center of the band gap has a charge of –1, while N_BV_N is neutral. During annealing or electron irradiation (Petrov et al. 2023), ionization of the vacancy is possible, so several processes leading to the transformation between V_B and N_BV_N are possible:

(0) V_B^{-1}–V_B^0 transition (blue arrow in Fig. 3(a)) — this transition is the ionization and a starting point for processes (1) and (2).

(1) V_B^0–$N_BV_N^0$ transition (orange arrow in Fig. 3(a)).

(2) Transition from V_B^0 (dotted line in Fig. 3(a)) in the atomic positions corresponding to the optimized charge state V_B^{-1} to $N_BV_N^0$ (purple arrow in Fig. 3(a)) — transition without relaxation, which might take place immediately after ionization, when the atomic structure has not relaxed yet.

In addition to the process described above, a transition without ionization is also possible:

(3) V_B^{-1}–$N_BV_N^{-1}$ transition (bright-green arrow in Fig. 3(a)).

And then, after the ionization, the system comes to the same neutral N_BV_N:

(4) $N_BV_N^{-1}$–$N_BV_N^0$ transition (dark-green arrow in Fig. 3(a)).

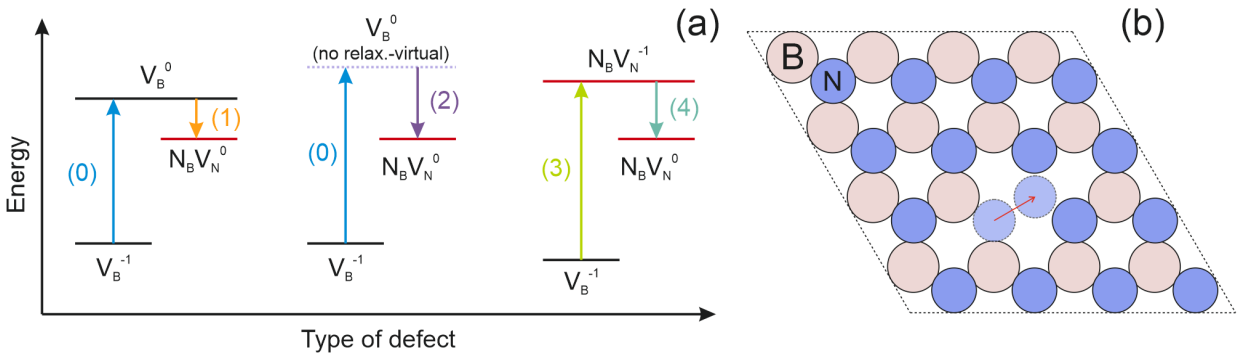

Fig. 3. (a) Schematic representation of transitions; (b) schematic representation of V_B–N_BV_N transformation

Considering the initial and final states for the processes (1), (2) and (3) mentioned above, we can calculate the transition barriers between different types of defects (Fig. 4).

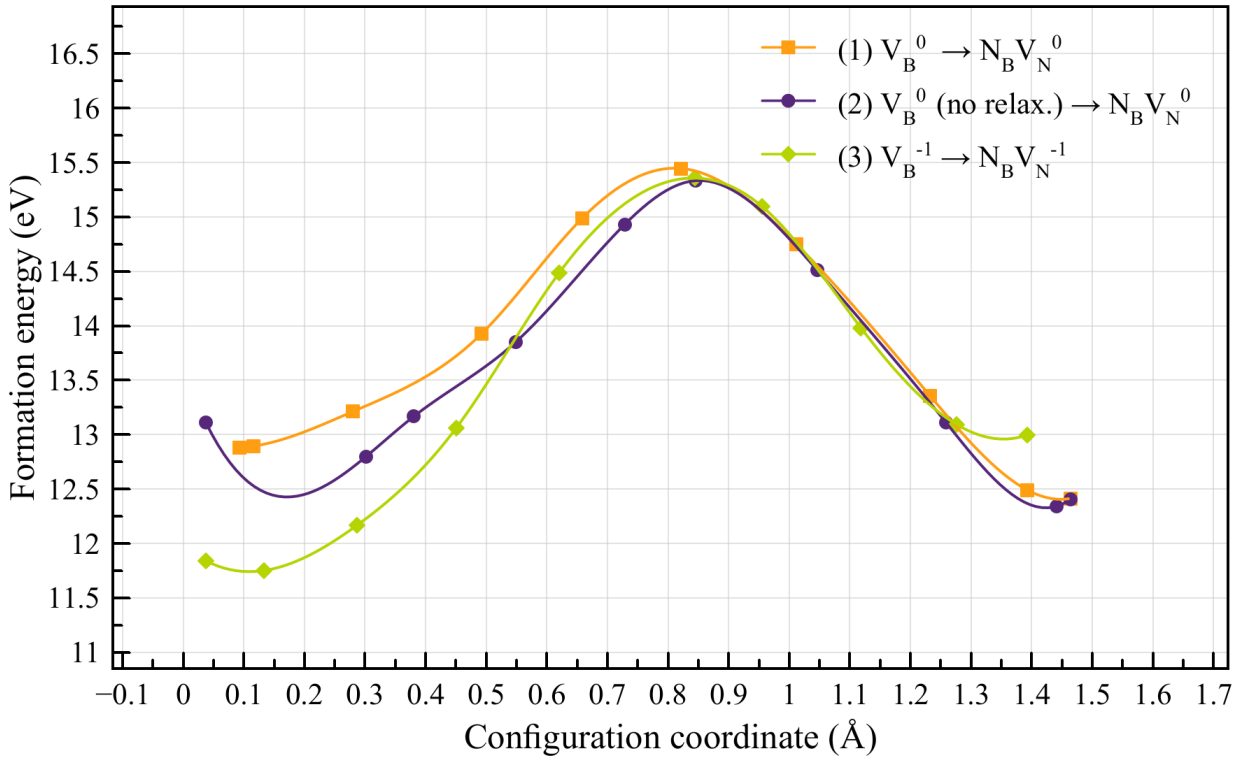

Fig. 4. Transition barriers between V_B and N_BV_N. Zero configuration coordinate corresponds to V_B

Based on the obtained barrier values using formulas (2) and (3), we can calculate the transition probabilities and annealing temperatures for forward (V_B to N_BV_N) and reverse (N_BV_N to V_B) transitions. The results are presented in Table 2.

 https://www.doi.org/10.33910/2687-153X-2024-5-4-215-220

Table 2. The values of the forward (E_f) and reverse (E_r) transition barriers (1) – (3), along with the calculated transition probabilities and annealing temperatures

Type of transition	E_f, eV	E_r, eV	Γ_f, s^{-1}	Γ_r, s^{-1}	T_f, K	T_b, K
(1)	2.57	3.03	2.76×10^{-31}	2.13×10^{-39}	923	1091
(2)	2.22	2.93	2.41×10^{-25}	–	800	–
(3)	3.52	2.36	8.33×10^{-48}	9.66×10^{-28}	1265	849

As shown in Table 2, the barrier for the transition from V_B to N_BV_N in the neutral state is lower than in the negatively charged state, but in all cases exceeds 2 eV, and the transition probabilities at room temperature are negligible. This indicates that to create N_BV_N–type defects from V_B, the structure must be provided with sufficient energy, such as through heating. The obtained annealing temperatures for the transitions are consistent with experimental results (Grosso et al. 2017; Tran et al. 2016; Venturi et al. 2024). Additionally, since the barrier for the reverse transition (3) is lower than that for the forward transition, the probability of the transformation from N_BV_N to V_B in the negatively charged state is quite high.

Conclusions

In this work, we calculated the formation energy of V_B and N_BV_N in different charge states for h-BN using the DFT method. The obtained values allowed us to consider transitions between defects and calculate their barriers. The latter were used to calculate the annealing temperatures and transition probabilities at room temperature. We assume that the process of defect transformation at room temperature observed in the work (Petrov et al. 2023) can be caused by the recombination of nonequilibrium excess charge carriers excited during electron irradiation. To complete the description of the studied processes, ionization processes should be considered in more detail. Therefore, we plan to continue investigating the ionization energies of V_B and N_BV_N further.

Conflict of Interest

The authors declare that there is no conflict of interest, either existing or potential.

Author Contributions

All the authors discussed the final work and took an equal part in writing the article.

References

Cassabois, G., Valvin, P., Gil, B. (2016) Hexagonal boron nitride is an indirect bandgap semiconductor. *Nature Photonics*, 10 (4), 262–266. https://doi.org/10.1038/nphoton.2015.277 (In English)

Dean, C. R., Young, A. F., Meric, I. et al. (2010) Boron nitride substrates for high-quality graphene electronics. *Nature Nanotechnology*, 5 (10), 722–726. https://doi.org/10.1038/nnano.2010.172 (In English)

Freysoldt, C., Neugebauer, J., van de Walle, C. G. (2011) Electrostatic interactions between charged defects in supercells. *Physica Status Solidi B*, 248 (5), 1067–1076. https://doi.org/10.1002/pssb.201046289 (In English)

Geick, R., Perry, C. H., Rupprecht, G. (1966) Normal modes in hexagonal boron nitride. *Physical Review*, 146 (2), article 543. https://doi.org/10.1103/PhysRev.146.543 (In English)

Grosso, G., Moon, H., Lienhard, B. et al. (2017) Tunable and high-purity room temperature single-photon emission from atomic defects in hexagonal boron nitride. *Nature Communications*, 8 (1), article 705. https://doi.org/10.1038/s41467-017-00810-2 (In English)

Larsen, A. H., Mortensen, J. J., Blomqvist, J. (2017) The atomic simulation environment—a Python library for working with atoms. *Journal of Physics: Condensed Matter*, 29 (27), article 273002. https://doi.org/10.1088/1361-648X/aa680e (In English)

Lindgren, P., Kastlunger, G., Peterson, A. A. (2019) Scaled and dynamic optimizations of nudged elastic bands. *Journal of Chemical Theory and Computation*, 15 (11), 5787–5793. https://doi.org/10.1021/acs.jctc.9b00633 (In English)

Liu, G-L., Wu, X-Y., Jing, P-T. et al. (2024) Single photon emitters in hexagonal boron nitride fabricated by focused helium ion beam. *Advanced Optical Materials*, 12 (9), article 2302083. https://doi.org/10.1002/adom.202302083 (In English)

Mortensen, J. J., Larsen, A. H., Kusima, M. et al. (2024) GPAW: An open python package for electronic structure calculations. *The Journal of Chemical Physics*, 160 (9), article 092503. https://doi.org/10.1063/5.0182685 (In English)

Pazos, S., Shen, Y., Zhang, H. et al. (2024) Memristive circuits based on multilayer hexagonal boron nitride for millimetre-wave radiofrequency applications. *Nature Electronics*, 7 (7), 557–566. https://doi.org/10.1038/s41928-024-01192-2 (In English)

Perdew, J. P., Burke, K. Ernzerhof, M. (1996) Generalized gradient approximation made simple. *Physical Review Letters*, 77 (18), 3865–3868. https://doi.org/10.1103/PhysRevLett.77.3865 (In English)

Petrov, Yu. V., Gogina, O. A., Vyvenko, O. F. et al. (2023) Effect of combined ion and electron irradiation on 2 eV luminescence band in hexagonal boron nitride. *Technical Physics*, 68 (7), 856–862. https://doi.org/10.61011/TP.2023.07.56627.62-23 (In English)

Tran, T. T., Bray, K., Ford, M. J. et al. (2016) Quantum emission from hexagonal boron nitride monolayers. *Nature Nanotechnology*, 11 (1), 37–41. https://doi.org/10.1038/NNANO.2015.242 (In English)

Venturi, G., Chiodini, S., Melchioni, N. et al. (2024) Selective generation of luminescent defects in hexagonal boron nitride. *Laser & Photonics Reviews*, 18 (6), article 2300973. https://doi.org/10.1002/lpor.202300973 (In English)

Weston, L., Wickramaratne, D., Mackoit, M. et al. (2018) Native point defects and impurities in hexagonal boron nitride. *Physical Review B*, 97 (21), article 214104. https://doi.org/10.1103/PhysRevB.97.214104 (In English)